OPEN ACCESS

Japanese Journal of Applied Physics **61**, 082004 (2022) **REGULAR PAPER**

https://doi.org/10.35848/1347-4065/ac7e10

Design of an ultra-sensitive and miniaturized diamond NV magnetometer based on a nanocavity structure

Ryota Katsumi[1,2*], Masaki Sekino[2], and Takashi Yatsui[1,2]

[1]*Graduate School of Engineering, Toyohashi University of Technology, 1-1 Hibarigaoka, Tempaku-cho, Toyohashi, Aichi 441-8580 Japan*
[2]*Graduate School of Engineering, the University of Tokyo, 7-3-1 Hongo, Bunkyo-ku, Tokyo 113-8656, Japan*

[*]E-mail: katsumi.ryota.ti@tut.jp

Received May 31, 2022; accepted July 3, 2022; published online July 19, 2022

The ensemble of nitrogen-vacancy (NV) centers in diamond allows for the potential realization of the sensitive magnetometers by leveraging their excellent spin properties. However, the NV-based magnetometers are limited by their experimental magnetic field sensitivity owing to its inefficient photon collection. Moreover, they are a disadvantage to the reduced spatial resolution and excessive excitation power. To overcome these issues, we propose a ultra-sensitive diamond magnetometer based on nanocavities. The device structure can attain a high collective efficiency and enhance the photon emission intensity of the NV ensemble. This device can allow the efficient photon collection even when considering the positional distribution of the NV centers. Our theoretical analysis indicates that the minimum expected sensitivity is 60 fT/$\sqrt{\mathrm{Hz}}$. The proposed design can achieve a volume-normalized sensitivity of 0.92 aT/$\sqrt{\mathrm{Hz\ cm^{-3}}}$ along with the required power of 7 μW, both of which are superior to those of bulk diamond. The proposed approach offers a promising route towards highly sensitive and energy-efficient magnetometers.

1. Introduction

Negatively charged nitrogen-vacancy (NV) centers in diamond have drawn a considerable interest as a promising candidate for a quantum sensor by virtue of their outstanding spin property.[1)] Because, the electron spins in the NV centers are optically accessible at room temperature to initialize and read out the quantum state with long coherence time. NV centers also allows the sensitive detection of various environmental parameters, including magnetic field, electric field, pressure, and temperature.[2–5)] Particularly, NV center ensembles have been intensively investigated as sensitive magnetic sensors with high spatial resolution,[4,6–8)] the sensitivity of which is theoretically compared with that based on current state-of-the-art magnetometers such as superconducting quantum-interference devices (SQUIDs) and atomic vapor cells (AVCs).[9)] The magnetic sensitivity of pT/$\sqrt{\mathrm{Hz}}$ under ambient conditions have been demonstrated using NV centers in bulk diamond.[10)]

Despite their tremendous progress, the experimental field sensitivity of NV-based magnetometers is lower than that of conventional magnetometers in several orders of magnitude.[1,11)] One of the critical factors, degrading the sensitivity of diamond magnetometers is the low collection efficiency of photons emitted from NV centers,[12)] where the extraction of photons from a diamond is hindered by the total internal reflections caused by its high refractive index ($n = 2.4$). For example, in conventional NV magnetometry, the photons emitted from NV centers in bulk diamond is collected via oil-immersion or air microscope objectives, resulting in a typical collective efficiency of $<10\%$.[13)] Several studies have been conducted to improve the photon collective efficiency of diamond magnetometers using the side collection method,[13)] a parabolic concentrator,[10)] coupling prisms,[14)] and dielectric gratings.[15)] Nevertheless, the reported photon collective efficiency is still below 50%. These bulk approaches also rely on the large sensing volume of NV centers to enhance the magnetic field sensitivity with excessive excitation laser power, thereby relinquishing the spatial resolution and hindrance to the miniaturization of the diamond magnetometers for practical applications.

Alternatively, the use of nanostructures allows for efficient photon collection and device miniaturization. To date, various types of nanophotonic components, such as photonic wire waveguides, ring resonators, and photonic crystals, have been successfully demonstrated in diamond photonics owing to the recent development of diamond nanofabrication technology.[16–21)] In this work, we propose a nanocavity-based diamond structure as a highly sensitive diamond magnetometer. The use of nanocavities enables the confinement and extraction of the NV photons radiated by the NV center ensemble together with the Purcell enhancement, which is an advantage for the efficient use of these photons. We demonstrate that the proposed configuration can attain photon collective efficiency exceeding 80%, and efficient photon collection is possible even when taking into account the actual positional distribution of NV centers. By theoretically analyzing the Purcell-enhanced NV emission, we showed that the minimum magnetic sensitivity of the proposed single cavity (multiple cavities) is 600 (60) fT/$\sqrt{\mathrm{Hz}}$. The small sensing volume of the device allows us to achieve a volume-normalized sensitivity of 0.92 aT/$\sqrt{\mathrm{Hz\ cm^{-3}}}$ along with the required pump power of approximately 7 μW. The designed structure can be combined with the current cutting-edge, electronic and photonic technology to construct a miniature and scalable device, with the potential for the realization of a highly sensitive, user-friendly, and energy-efficient diamond magnetic sensor.

2. Device design

Figure 1(a) illustrates the device structure that was investigated in this study. The NV centers are uniformly distributed in the air-bridged diamond nanobeam. We formed a Fabry–Perot cavity inside the waveguide by implementing photonic

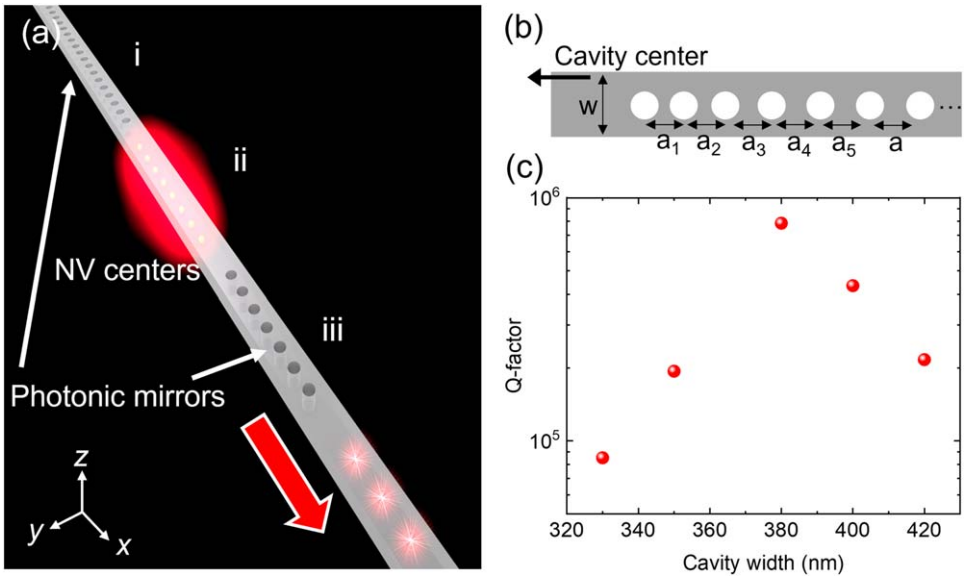

Fig. 1. (Color online) (a) Schematic device structure that was investigated in this study. (b) Schematic photonic mirrors in our diamond nanobeam cavity. (c) Calculated Q-factors as a function of the cavity width.

crystal mirrors on both the edges of the diamond waveguide. The photons emitted from the NV centers first couple with the investigated cavity resonant mode at the wavelength of the zero-phonon line (ZPL, 637 nm). The cavity mode is then coupled to the guided mode as shown by the red arrow in Fig. 1(a). Notably, by controlling the number of holes in the right photonic mirror [Sect. iii in Fig. 1(a)], the cavity resonant mode can be in unidirectional waveguide,[22] allowing the exploitation of most of the NV photons.

The coupling efficiency of the cavity mode to the waveguide propagating mode is given by the ratio of the waveguide mode compared to the free space scattering as follows:

$$\eta_{\mathrm{cav}} = \frac{\frac{1}{Q_{\mathrm{wg}}}}{\frac{1}{Q_{\mathrm{wg}}} + \frac{1}{Q_{\mathrm{fs}}}}, \tag{1}$$

where Q_{wg} is the Q-factor characterizing the coupling between the cavity mode and waveguide mode and Q_{fs} is related to the light leakage of the cavity mode in free space. The reflectivity of the photonic crystal mirrors depends on the number of holes (N), thus Q_{wg} can be controlled by adjusting N. On the other hand, Q_{fs} is related to the out-of-plane photon loss. We can simulate Q_{fs} by conducting a three-dimensional finite difference time domain (FDTD) simulation, considering the situation when $Q_{\mathrm{fs}} \gg Q_{\mathrm{wg}}$ with large N. We have set the lattice period of the photonic mirrors and slab thickness to be 218 nm and 130 nm, respectively in order to investigate the TE cavity mode resonating at the ZPL of 637 nm. The air holes near the cavity region are gradually modulated to minimize the cavity loss as shown in Fig. 1(b) ($a_1 = 0.8400a$, $a_2 = 0.8464a$, $a_3 = 0.8656a$, $a_4 = 0.8976a$, and $a_5 = 0.9424a$).[23,24] The cavity length was 48 μm, yielding 2.4×10^4 NV centers inside the single cavity for NV centers with a density of $D_{\mathrm{NV}} = 1 \times 10^{16}$ cm^{-3}. Figure 1(c) shows the calculated Q_{fs} as a function of the cavity width (w). It can be seen that Q_{fs} reaches 8×10^6 for $w = 380$ nm. We note that the calculated Q-factors will be within the technological reach since the current fabrication technology of diamond photonics allows for a disk cavity with an ultra-high Q-factor of over 3×10^5.[21]

We optimized the cavity structure to achieve the near-unity collective efficiency of the emission of NV center ensembles. The coupling efficiency of the NV dipole emission and the investigated cavity resonant mode is expressed as follows:

$$\beta_{\mathrm{NV}} = \frac{F_{\mathrm{ZPL}}\gamma_{\mathrm{ZPL}}}{F_{\mathrm{ZPL}}\gamma_{\mathrm{ZPL}} + \gamma_{\mathrm{PSB}}} = \frac{F}{F+1}, \tag{2}$$

where γ_{ZPL} (γ_{PSB}) is the spontaneous emission rate in the ZPL (phonon sideband). For this discussion, we define the Purcell factor F (overall spontaneous emission rate enhancement) as

$$F = F_{\mathrm{ZPL}}\mathrm{DW} = \frac{3}{4\pi^2}\frac{Q}{V_{\mathrm{mode}}}\left(\frac{\lambda}{n}\right)^3 \times \mathrm{DW}, \tag{3}$$

where F_{ZPL} is the spectrally resolved spontaneous emission rate enhancement, Q is the Q-factor of the investigated cavity, V_{mode} is the mode volume of the investigated cavity mode, n is the effective refractive index, and $\mathrm{DW} = \frac{\gamma_{\mathrm{ZPL}}}{\gamma_{\mathrm{ZPL}} + \gamma_{\mathrm{PSB}}} (=0.05)$ is the Debye–Waller factor. The higher F allows the suppression of the phonon sideband emission,[25] and the cavity structure enables the ZPL emission to efficiently couple with the cavity resonant mode. Our object is to collect the whole of the NV emission, thus, we can focus on enhancing the overall spontaneous emission rate by coupling all the emission into the ZPL. Importantly, most of the studies reported in the literature regarding the Purcell enhancement of the NV emission are concerned with F_{ZPL} rather than F.[17,19]

Figure 2(a) summarizes the simulated Q-factors (Q_{wg}), coupling efficiencies, and the total output efficiencies ($\eta_{\mathrm{cav}} \times \beta_{\mathrm{NV}}$) as a function of the number of holes (N). In this study, η_{cav} is calculated by using Eq. (1). We deduced β_{NV} using the simulated values of the Q-factors in Eqs. (2) and (3). The FDTD calculations revealed that Q_{wg} is exponentially reduced with decreasing N owing to the efficient coupling of the cavity resonant mode and the waveguide mode. The

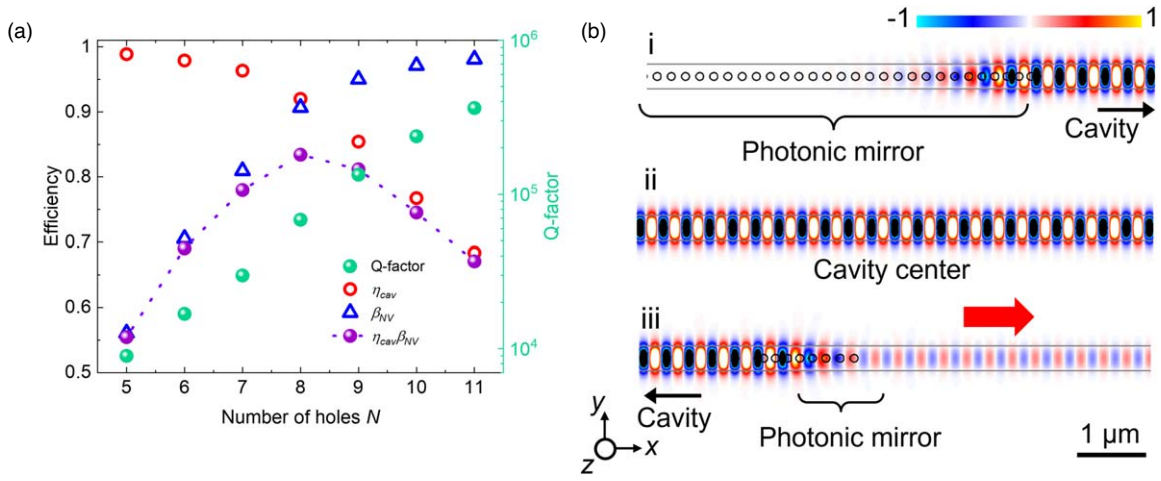

Fig. 2. (Color online) (a) Simulated Q-factors (Q_{wg}), coupling efficiencies, and total output efficiencies are shown as a function of N. Green: Q-factors, Red: $\boldsymbol{\eta_{cav}}$, Blue: $\boldsymbol{\beta_{NV}}$, Purple: total output efficiency calculated as $\boldsymbol{\eta_{cav}} \times \boldsymbol{\beta_{NV}}$. (b) Electric field distributions (E_y component) of the cavity resonant mode in Sects. ii of Fig. 1(a).

increase in η_{cav}, that accompanied the reduction of N from 11 to 5 corresponds to the exponential decay of Q_{wg}. When $N = 8$, we obtained $\eta_{cav} = 0.91$, $Q_{wg} = 6.8 \times 10^4$, and $V_{mode} = 0.5\ \mu m^3$. Despite the extreme reduction of Q_{wg}, which may lead to the degradation of the emitter-cavity coupling β_{NV}, we achieved the highest total output efficiency $\eta_{cav} \times \beta_{NV}$ of 0.83 with the maximum Purcell factor of $F = 9.7$. Figure 2(b) shows the electric field distribution (E_y component) of the cavity resonant mode in each section of Fig. 1(a). The light is perfectly reflected in Sect. i of Fig. 1(a), and surely confined in the cavity center in Sect. ii. For Sect. iii, the photons inside the cavity indeed propagated unidirectionally. We can also confirm that light scattering did not occur in any of the sections, suggesting that the proposed structure allows for the efficient use of photons.

In the above discussion, we assume that all the NV centers are perfectly positioned at the field are maximum at the investigated cavity resonant mode. To consider the actual uniform distribution of the NV centers inside the cavity, we evaluated the position-dependent coupling efficiency from the electric field distribution. In the event of any misalignment of the position and orientation of the dipole source, the Purcell factor of Eq. (3) is modified as follows:

$$F = F^{max} \times \frac{|d(r) \cdot E(r)|^2}{|d(r)|^2 |E_{max}|^2}, \tag{4}$$

where F^{max}(=9.7) is the maximum Purcell factor, $\boldsymbol{d}(\boldsymbol{r})$ is the dipole moment, $\boldsymbol{E}(\boldsymbol{r})$ is the amplitude of the electric field at position $\boldsymbol{r}$, and $\boldsymbol{E_{max}}$ is the maximum amplitude of $\boldsymbol{E}(\boldsymbol{r})$. Figures 3(a) and 3(b) display color maps of β_{NV} in the xy and zx plane around the cavity center calculated using Eqs. (2) and (3). Although β_{NV} significantly decreases at the antinode positions ($x = \pm 90$, ± 260 nm), high values of β_{NV} ($\geqslant 0.7$) are sustained in 45% of the diamond nanobeam in Fig. 3(a). We also confirm that $\beta_{NV} \geqslant 0.7$ for the zx plane of Fig. 3(b) is because of the strong light confined along the z-axis. Thus, we define the effective number of NV centers with $\beta_{NV} \geqslant 0.7$ ($F \geqslant 2.3$) that can contribute to optically detect the magnetic resonances (ODMR) measurement as $n_{NV} = 0.45 D_{NV} V$, where V is the volume of the investigated cavity (see also Appendix A).

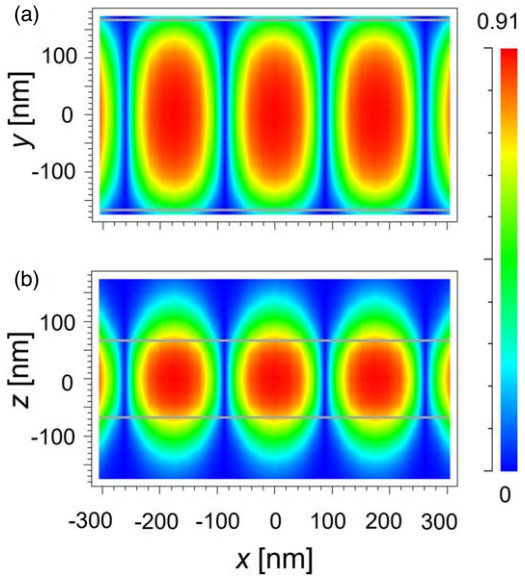

Fig. 3. (Color online) (a) and (b) Color map of the calculated $\boldsymbol{\beta_{NV}}$ around the cavity center of Sect. ii in Fig. 1(a) [(a): xy plane, (b): zx plane]. (c) Output efficiency of the dipole radiation as a function of the dipole positions along the x-direction.

3. Evaluation

We evaluated the magnetic sensitivity of the proposed device structure. The ac magnetic sensitivity of NV center ensembles is expressed as follows:[1)]

$$\delta B = \frac{\pi}{2} \frac{\hbar}{g \mu_B} \frac{\sqrt{T_m}}{C \sqrt{\eta_{total} \times F n_{NV} N_{photon} \times T_2}}, \tag{5}$$

where $\hbar$ is the Planck constant, $g \approx 2$ is the electronic g-factor, μ_B is the Bohr magneton, T_m is the measurement time, T_2 is the spin coherence time, C is the ODMR contrast, and N_{photon} is the number of photons detected from a single NV center. Using the previously reported photon count rate of 1.0×10^5 counts per second (cps) for a single NV in isotopically pure diamond[26)] with a typical collective efficiency of up to 5%,[13)] we estimate $N_{photon}/T_m = 2.0 \times 10^6$ cps. We also employ $F = 2.3$ and $\beta_{NV} = 0.7$ in the analysis below. Details of the analysis are shown in Appendix B.

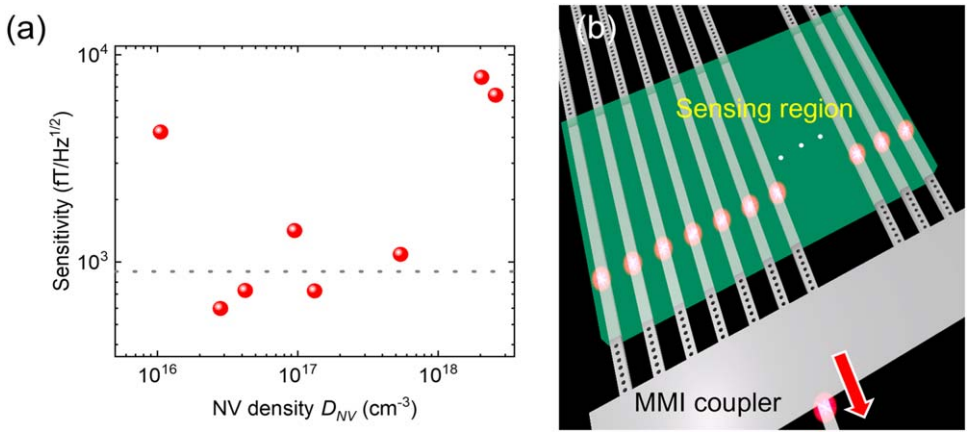

Fig. 4. (Color online) (a) Calculated ac magnetic sensitivity as a function of the NV density. (b) Schematics of the arrayed nanocavities for improving the sensitivity of the magnetometer.

Table I. Values of volume-normalized sensitivity, sensing volume, and required pump power of diamond NV magnetometers.

	Bulk diamond (theory)[1)]	Bulk diamond (experiment)[10)]	Single nanocavity (this study)
Sensing volume	3 mm^3	8.5×10^{-4}mm^3	2.4 μm^3
Volume-normalized sensitivity	250 aT/$\sqrt{\text{Hz}}$ cm^{-3}	830 aT/$\sqrt{\text{Hz}}$ cm^{-3}	0.92 aT/$\sqrt{\text{Hz}}$ cm^{-3}
Required pump power	140 W	0.4 W	7 μW

Figure 4(a) shows the expected magnetic sensitivity calculations using Eq. (5) as a function of the NV density (D_{NV}). The values of T_2 for each D_{NV} are adapted from a previous study.[27)] We confirmed that the magnetic sensitivity is less than 1 pT/$\sqrt{\text{Hz}}$ at approximately $D_{\text{NV}} = 2.8 \times 10^{16}$ cm^{-3}, which is below the minimum experimentally achieved value of 0.9 pT/$\sqrt{\text{Hz}}$ (indicated by the dashed line in Fig. 4(a)].[10)] For $D_{\text{NV}} = 2.8 \times 10^{16}$ cm^{-3} along with the reported T_2 of 250 μs,[27)] the sensitivity of our single diamond nanocavity is expected to be 600 fT/$\sqrt{\text{Hz}}$. The degradation of the sensitivity for $D_{\text{NV}} > 1.0 \times 10^{18}$ cm^{-3} is attributed to the optical absorption loss and reduction of the T_2 coherence time due to the high NV density. For high-resolution magnetic sensing, the evaluation of the magnetic sensitivity by normalizing the sensing volume of the magnetometer is crucial. Owing to the small sensing volume (i.e. the cavity size of $V = 2.4$ μm^3), the volume-normalized sensitivity of the proposed single cavity is 0.92 aT/$\sqrt{\text{Hz}}$ cm^{-3} for $D_{\text{NV}} = 2.8 \times 10^{16}$ cm^{-3}, which is three orders of the magnitude higher than those based on bulk diamond approaches of 850 aT/$\sqrt{\text{Hz}}$ cm^{-3} (shown by the gray dotted curve).

The magnetic sensitivity can be further improved when the number of nanocavities are increased by arraying the cavities as shown in Fig. 4(b). The photons from each cavity can be collected from a single waveguide, for example, by connecting each cavity to the multi-mode interference (MMI) coupler. For 100 arrayed cavities, the minimum sensitivity is expected to be 60 fT/$\sqrt{\text{Hz}}$, demonstrating the ultra-high magnetic sensitivity in comparison to that of SQUIDs and AVCs.[11)]

The current magnetometer based on bulk diamond requires excessive input laser power (several watts) due to the the large excitation volume ($\sim 10^{-4}$ mm^3). In contrast, our proposed device has the potential for low power excitation by virtue of the small excitation volume. Table I summarizes the values of the sensing volume, volume-normalized magnetic sensitivity, and the required pump power of the diamond NV magnetometer based on the bulk diamond and our single cavity. The theoretical and experimental values of bulk diamond are adopted from previous studies.[1,10)] We also evaluate the required pump power by comparing the sensing volume with that of bulk diamond.[15)] For the waveguide-based structure, the pump laser can be coupled with the device efficiently using an adiabatic spot size converter[28)] or Bragg grating.[29)] Because the transmission ratio of a 532 nm excitation laser is calculated to be 0.3 for the photonic crystal mirror of $N = 8$, the required pump power of the proposed nanocavity structure is estimated as 7 μW, which is more than four orders of magnitude superior to those based on bulk diamond approaches.

4. Conclusion

In summary, we demonstrated a nanocavity-based diamond structure for ultra-sensitive magnetic sensors. We verified that the proposed configuration can attain near-unity collective efficiency of the photon emission emitted from NV centers. The device can achieve such high output efficiency even when considering the actual positional distribution and dipole orientation of the the NV centers. The minimum sensitivity of the proposed structure is 600 fT/$\sqrt{\text{Hz}}$ with further improvement to 60 fT/$\sqrt{\text{Hz}}$ by arraying the nanocavities. The small sensing volume of the design can provide volume-normalized sensitivity of 0.92 aT/$\sqrt{\text{Hz}}$ cm^{-3}, which represents an improvement of three orders of magnitude over previous NV diamond magnetometers. In addition, the required power of the excitation laser is drastically reduced from several watts to approximately 7 μW. These nanocavities can be combined with existing cutting-edge electronic and photonic technology for building miniature and scalable

devices. The proposed approach potentially allows for a highly sensitive, compact, and energy-efficient diamond magnetometer.

Acknowledgments

This work was supported by MEXT Q-LEAP of Grant Number JPMXS0118067395 and Kakenhi (18H01470, 20H02197, 20H05091, 20K21118, 21K20428, 22H01525, 22K14289).

Appendix A

To further confirm that our design is robust against the positional distribution of NV centers, we directly simulated the output efficiency using a point dipole emitter oscillating in the y-direction. In the simulation, the NV center was assumed to be a dipole source oscillating along the y-axis with the wavelength of 637 nm at $y = 0$ nm and $z = 0$ nm. Figure A·1 shows the output efficiency of the dipole radiation as a function of the dipole position along the x-direction. Except for the dipole position of 90 nm, an output efficiency of approximately 70% is supported. It should be noted that these simulations only focus on the ZPL emission (i.e. F_{ZPL}), and the output efficiency based on a dipole source is not equal to $\eta_{\mathrm{cav}} \times \beta_{\mathrm{NV}}$. However, these results indicate that our proposed structure enables efficient photon collection from NV center ensembles even while considering their positional distribution inside the cavity.

Appendix B

Since the cavity contains a high density of NV ensembles, the optical absorption by the NV centers should be considered in the analysis of the sensitivity. Thus, we modify the total output efficiency of the NV emission as follows:

$$\eta_{\mathrm{total}} = \frac{\frac{1}{Q_{\mathrm{wg}}}}{\frac{1}{Q_{\mathrm{wg}}} + \frac{1}{Q_{\mathrm{abs}}} + \frac{1}{Q_{\mathrm{fs}}}} \times \beta_{\mathrm{NV}}, \tag{6}$$

where $Q_{\mathrm{abs}} = \frac{2\pi n}{\alpha\lambda}$ (α: absorption constant) is the Q-factor related to the optical absorption. Previously, the absorption constant was reported to be $\alpha = 0.45\,\mathrm{cm}^{-1}$ for the NV density of 2.3×10^{16} cm^{-3}.[6] We assume Q_{abs} is simply determined by the absorption constant and the NV density.

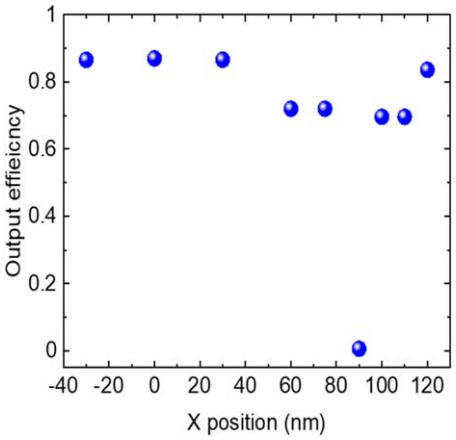

Fig. A·1. (Color online) Output efficiency of the dipole radiation as a function of the dipole positions along the x-direction.

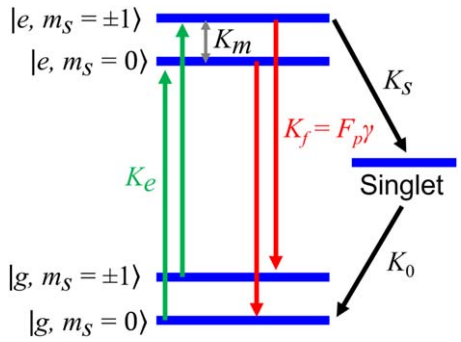

Fig. A·2. (Color online) Energy levels and allowed transitions for the NV center with nonradiative spin-mixing transitions in the excited state.

Reportedly, the ODMR contrast may be affected by the Purcell enhancement.[30] To evaluate C, we conducted a theoretical analysis of the NV dynamics with the Purcell effect in accordance with previous studies.[30] Figure A·2 shows the energy levels and allowed transitions for the NV center with nonradiative spin-mixing transitions in the excited state. We denote the ground (excited) states of the NV spin $m_{\mathrm{s}} = 0$ and $m_{\mathrm{s}} = \pm 1$ as $|g,\ m_{\mathrm{s}} = 0\rangle$ ($|e,\ m_{\mathrm{s}} = 0\rangle$) and $|g,\ m_{\mathrm{s}} = \pm 1\rangle$ ($|e,\ m_{\mathrm{s}} = \pm 1\rangle$), respectively. By assuming a simple situation where the spin-mixing induced by the off-axis magnetic field is the same for excitation and emission, the rate equations are expressed as follows:

$$\begin{aligned}
P'_{\mathrm{g0}}(t) &= -K_{\mathrm{e}}P_{\mathrm{g0}}(t) + K_{\mathrm{f}}P_{\mathrm{e0}}(t) + K_0P_{\mathrm{s}}(t),\\
P'_{\mathrm{g1}}(t) &= -K_{\mathrm{e}}P_{\mathrm{g1}}(t) + K_{\mathrm{f}}P_{\mathrm{e1}}(t),\\
P'_{\mathrm{e0}}(t) &= K_{\mathrm{e}}P_{\mathrm{g0}}(t) - (K_{\mathrm{f}} + 2K_{\mathrm{m}})P_{\mathrm{e0}}(t) + K_{\mathrm{m}}P_{\mathrm{e1}}(t),\\
P'_{\mathrm{e1}}(t) &= K_{\mathrm{e}}P_{\mathrm{g1}}(t) - (K_{\mathrm{f}} + K_{\mathrm{s}} + K_{\mathrm{m}})P_{\mathrm{e1}}(t) + 2K_{\mathrm{m}}P_{\mathrm{e0}}(t),\\
P'_{\mathrm{s}}(t) &= K_{\mathrm{S}}P_{\mathrm{e1}}(t) - K_0P_{\mathrm{s}}(t),
\end{aligned} \tag{7}$$

where K_{e} is the spin-preserving excitation rate, $K_{\mathrm{f}} = F\gamma$ is the Purcell-enhanced decay rate (γ: spin-preserving excitation emission rate), K_{m} is the rate of the spin-mixing transitions, K_{s} is the transition rate from $|e,\ m_{\mathrm{s}} = \pm 1$ to the singlet state, and K_0 is the transition rate from the singlet state to $|g,\ m_{\mathrm{s}} = 0\rangle$. In the following analysis, we employ the typical rates of the NV centers: $\gamma = 690$ MHz, $K_{\mathrm{m}} = 3.1$ MHz, $K_{\mathrm{s}} = 51$ MHz, and $K_0 = 3.3$ MHz. We also assume the photoluminescence saturation regime,[30] i.e. $K_{\mathrm{e}} = 2K_{\mathrm{f}}$. To evaluate C, we introduce the signal-to-noise (SNR) ratio as follows:

$$\mathrm{SNR} = \frac{N_0 - N_1}{\sqrt{N_0 + N_1}}, \tag{8}$$

where N_0 and N_1 are the expectation values of the detected number of photons during the realistic measurement time: $T = 260$ ns for $m_{\mathrm{s}} = 0$ and $m_{\mathrm{s}} = \pm 1$, respectively. The relationship between the contrast value and SNR is as follows:

$$\sqrt{F} \times \frac{C}{C(F=1)} = \frac{\mathrm{SNR}(F)}{\mathrm{SNR}(F=1)}. \tag{9}$$

Using the calculated values $\mathrm{SNR}(F) = 2.1$ and $\mathrm{SNR}(F = 1) = 1.4$, together with the typical value $C(F = 1) = 0.20$, we obtained $C = 0.202$ for $F = 2.3$. We can confirm that the

contrast value by itself changed slightly as a result of the Purcell effect, and this result agrees well with the discussion in a previous study.[30)]

ORCID iDs

Ryota Katsumi https://orcid.org/0000-0002-5681-7621
Takashi Yatsui https://orcid.org/0000-0001-7295-4514

1) J. M. Taylor, P. Cappellaro, L. Childress, L. Jiang, D. Budker, P. R. Hemmer, A. Yacoby, R. Walsworth, and M. D. Lukin, Nat. Phys. **4**, 810 (2008).
2) Y. Wu, F. Jelezko, M. B. Plenio, and T. Weil, Angew. Chem. Int. Ed. Engl. **55**, 6586 (2016).
3) R. Schirhagl, K. Chang, M. Loretz, and C. L. Degen, Annu. Rev. Phys. Chem. **65**, 83 (2014).
4) A. Kuwahata et al., Sci. Rep. **10**, 2483 (2020).
5) T. Yanagi et al., ACS Nano **15**, 12869 (2021).
6) H. Clevenson, M. E. Trusheim, C. Teale, T. Schröder, D. Braje, and D. Englund, Nat. Phys. **11**, 393 (2015).
7) D. R. Glenn, D. B. Bucher, J. Lee, M. D. Lukin, H. Park, and R. L. Walsworth, Nature **555**, 351 (2018).
8) F. M. Stürner et al., Adv. Quantum Technol. **4**, 2000111 (2021).
9) C. L. Degen, F. Reinhard, and P. Cappellaro, Rev. Mod. Phys. **89**, 035002 (2017).
10) T. Wolf, P. Neumann, K. Nakamura, H. Sumiya, T. Ohshima, J. Isoya, and J. Wrachtrup, Phys. Rev. **5**, 041001 (2015).
11) J. Kitching, Appl. Phys. Rev. **5**, 031302 (2018).
12) J. F. Barry, J. M. Schloss, E. Bauch, M. J. Turner, C. A. Hart, L. M. Pham, and R. L. Walsworth, Rev. Mod. Phys. **92**, 015004 (2020).
13) D. Le Sage, L. M. Pham, N. Bar-Gill, C. Belthangady, M. D. Lukin, A. Yacoby, and R. L. Walsworth, Phys. Rev. B. **85**, 121202 (2012).
14) Z. Ma, S. Zhang, Y. Fu, H. Yuan, Y. Shi, J. Gao, L. Qin, J. Tang, J. Liu, and Y. Li, Opt. Express **26**, 382 (2018).
15) J. B. Zheng, A. C. Liapis, E. H. Chen, C. T. Black, and D. Englund, Opt. Express **25**, 32420 (2017).
16) M. J. Burek, N. P. de Leon, B. J. Shields, B. J. Hausmann, Y. Chu, Q. Quan, A. S. Zibrov, H. Park, M. D. Lukin, and M. Loncar, Nano Lett. **12**, 6084 (2012).
17) B. J. Hausmann et al., Nano Lett. **13**, 5791 (2013).
18) M. J. Burek, Y. Chu, M. S. Liddy, P. Patel, J. Rochman, S. Meesala, W. Hong, Q. Quan, M. D. Lukin, and M. Loncar, Nat. Commun. **5**, 5718 (2014).
19) L. Li et al., Nat. Commun. **6**, 6173 (2015).
20) B. Khanaliloo, M. Mitchell, A. C. Hryciw, and P. E. Barclay, Nano Lett. **15**, 5131 (2015).
21) M. Mitchell, D. P. Lake, and P. E. Barclay, APL Photonics **4**, 016101 (2019).
22) A. Enderlin, Y. Ota, R. Ohta, N. Kumagai, S. Ishida, S. Iwamoto, and Y. Arakawa, Phys. Rev. B **86**, 075314 (2012).
23) P. B. Deotare, M. W. McCutcheon, I. W. Frank, M. Khan, and M. Lončar, Appl. Phys. Lett. **94**, 121106 (2009).
24) Y. Ota, R. Ohta, N. Kumagai, S. Iwamoto, and Y. Arakawa, Phys. Rev. Lett. **114**, 143603 (2015).
25) D. Riedel, I. Söllner, B. J. Shields, S. Starosielec, P. Appel, E. Neu, P. Maletinsky, and R. J. Warburton, Phys. Rev. **7**, 2160 (2017).
26) I. Lovchinsky et al., Science **351**, 836 (2016).
27) O R. Rubinas, V. V. Vorobyov, V. V. Soshenko, S. V. Bolshedvorskii, V. N. Sorokin, A. N. Smolyaninov, V. G. Vins, A. P. Yelisseyev, and A. V. Akimov., J. Phys. Commun. **2**, 115003 (2018).
28) M. Pu, L. Liu, H. Ou, K. Yvind, and J. M. Hvam, Opt. Commun. **283**, 3678 (2010).
29) X. Zhou, I. Kulkova, T. Lund-Hansen, S. L. Hansen, P. Lodahl, and L. Midolo, Appl. Phys. Lett. **113**, 251103 (2018).
30) S. A. Wolf, I. Rosenberg, R. Rapaport, and N. Bar-Gill, Phys. Rev. B **92**, 235410 (2015).